Supplementary materials

MiR-205-5p and miR-342-3p cooperate in the repression of E2F1 in the context of anticancer chemotherapy resistance

Xin Lai[1,#,*], Shailendra K Gupta[2,6,#], Ulf Schmitz[3,4,#], Stephan Marquardt[5], Susanne Knoll[5], Alf Spitschak[5], Olaf Wolkenhauer[2,7,§], Brigitte M Pützer[5,§], Julio Vera[1,§]

[1]Laboratory of Systems Tumour Immunology, Department of Dermatology, Friedrich-Alexander-University of Erlangen-Nürnberg (FAU) and Universitätsklinikum Erlangen, Erlangen, Germany

[2]Department of Systems Biology and Bioinformatics, University of Rostock, Rostock, Germany

[3]Gene & Stem Cell Therapy Program, Centenary Institute, University of Sydney, Camperdown, Australia

[4]Sydney Medical School, University of Sydney, Camperdown, Australia

[5]Institute of Experimental Gene Therapy and Cancer Research, Rostock University Medical Centre, Rostock, Germany

[6]CSIR-Indian Institute of Toxicology Research, Lucknow, India

[7]Stellenbosch Institute for Advanced Study (STIAS), Wallenberg Research Centre at Stellenbosch University, Stellenbosch, South Africa

[#]Equal first authors

[§]Equal senior authors

[*]To whom correspondence should be addressed: Xin Lai, Tel: +49(0)91318545888, Fax: +49(0)91318533874, Email: xin.lai@uk-erlangen.de.

Table of contents

1. 3D structure modelling and molecular dynamics simulations

1.1. Three-dimensional model design

For the initial tertiary structure of the RNA triplexes ($mRNA_{E2F1}$/$miRNA_1$/$miRNA_2$) as well as their two intrinsic RNA duplexes ($mRNA_{E2F1}$/$miRNA_1$ and $mRNA_{E2F1}$/$miRNA_2$), we used the RNAComposer web server (1), a tool for constructing large RNA 3D structures based on user defined secondary structure information. We used the secondary structures of the RNA complexes and received initial 3D structures in the form of long concatenated mRNA and miRNA units. Then, we used the *Build and Edit Nucleic Acid* tool in BIOVIA® Discovery Studio 4.5 to separate RNA units present in the complex as per the procedure described in our previous publication (2). To further optimize the 3D structures of RNA complexes and to remove steric overlap that produces bad contacts we used *Smart Min*imizer protocol available in BIOVIA® Discovery Studio 4.5 after assigning the charmm27 force field, a superset of the charmm22 force field with the additional coverage for nucleic acids (3, 4).

The *Smart Minimizer* protocol was set for a maximum run of 5000 steps with the Minimization RMS Gradient tolerance of 0.1 kcal/(mol x Å) to terminate the minimization routine in case the average gradient is less than or equal to the set cut-off. After the structural optimization, we calculated initial potential energies of all the RNA complexes using the *Calculate Energy* protocol in BIOVIA® DS 4.5. Such energy profile indicates the stability of the RNA complexes in the 3D model.

1.2. Molecular dynamics simulations

Molecular dynamics simulations were carried out using the *Standard Dynamics Cascade* protocol in BIOVIA® DS 4.5 in four steps: (i) minimization; (ii) heating and cooling; (ii) equilibrium run; and (iv) production run, for all the potential cooperating miRNAs complexed with the 3' UTR of E2F1. Minimization of the 3D structures to find the most stable confirmations of the RNA

complexes was carried out using the Steepest Descent algorithm followed by the Conjugate Gradient algorithm for 2000 steps each. In case the structure was not minimized, the protocol was repeated iteratively. After the minimization step, all the complexes were subjected to gradual heating from 50 K to 300 K by rescaling the velocity of each atom in a total of 10,000 steps with the time interval of 1 fs. The initial velocity was assigned according to a Maxwell-Boltzmann distribution corresponding to a temperature close to 50 K. In the equilibration phase the system was stabilized around 300 K temperature by periodically reassigning the velocities to each atom employing the LeapFrog Verlet algorithm with time steps of 1 fs in 50,000 steps. After heating, RNA complexes were subjected to the production run at constant-temperature, constant-volume ensemble (NVT) for initially 500 ps. The production run was further extended in blocks of 100 ps for those RNA complexes where at least one miRNA was still attached to E2F1 mRNA. Trajectories of the atoms were recorded at each 1,000 steps to investigate intermolecular H-bonds during the course of simulation. All simulation steps were carried out in the Generalized Born with simple SWitching (GBSW) implicit solvent model with dielectric constant 80 for better approximation of the solvent effect on the RNA triplex. We have deliberately used the GBSW implicit solvent model to save computational cost, which arises due to the long chain-like structures of RNA complexes that require a large number of solvent molecules in case of explicit solvent models. The SHAKE algorithm constraint was set to true for all the covalent bonds involving hydrogen atoms at their respective distances from the charmm27 force field parameters.

2. Mathematical modelling of E2F1 regulation by miRNAs

2.1. Kinetic modelling of E2F1 repression efficiency in paired miRNA regulation

To elaborate on the mechanism by which E2F1 is repressed by cooperative miRNA pairs, we developed a kinetic model of ordinary differential equations.

$$\frac{\partial E2F1}{\partial t} = k_{prod}^{E2F1} \cdot mE2F1 - k_{deg}^{E2F1} \cdot E2F1 \tag{S1}$$

$$\frac{\partial mE2F1}{\partial t} = k_{prod}^{mE2F1} \cdot TF_{mE2F1} - k_{deg}^{mRE2F1}.mE2F1 - k_{ass}^{duplex_1} \cdot mE2F1 \cdot miRNA_1 - k_{ass}^{duplex_2} \cdot mE2F1 \cdot miRNA_2 - k_{ass}^{triplex} \cdot mE2F1 \cdot miRNA_1 \cdot miRNA_2 + k_{dis}^{duplex_1} \cdot duplex_1 + k_{dis}^{duplex_2} \cdot duplex_2 + k_{dis}^{triplex} \cdot triplex \tag{S2}$$

$$\frac{\partial miRNA_1}{\partial t} = k_{prod}^{miRNA_1} \cdot TF_{miRNA_1} + k_{dis}^{duplex_1} \cdot duplex_1 + k_{dis}^{triplex} \cdot triplex - k_{deg}^{miRNA} \cdot miRNA_1 - k_{ass}^{duplex_1} \cdot mE2F1 \cdot miRNA_1 - k_{ass}^{triplex} \cdot k_{ass}^{triplex} \cdot mE2F1 \cdot miRNA_1 \cdot miRNA_2 \tag{S3}$$

$$\frac{\partial miRNA_2}{\partial t} = k_{prod}^{miRNA_2} \cdot TF_{miRNA_2} + k_{dis}^{duplex_2} \cdot duplex_2 + k_{dis}^{triplex} \cdot triplex - k_{deg}^{miR342} \cdot miRNA_2 - k_{ass}^{duplex_2} \cdot mE2F1 \cdot miRNA_2 - k_{ass}^{triplex} \cdot k_{ass}^{triplex} \cdot mE2F1 \cdot miRNA_1 \cdot miRNA_2 \tag{S4}$$

$$\frac{\partial duplex_1}{\partial t} = k_{ass}^{duplex_1} \cdot mE2F1 \cdot miRNA_1 - k_{deg}^{duplex_1} \cdot duplex_1 - k_{dis}^{duplex_1} \cdot duplex_1 \tag{S5}$$

$$\frac{\partial duplex_2}{\partial t} = k_{ass}^{duplex_2} \cdot mE2F1 \cdot miRNA_2 - k_{deg}^{duplex_2} \cdot duplex_2 - k_{dis}^{duplex_2} \cdot duplex_2 \tag{S6}$$

$$\frac{\partial triplex}{\partial t} = k_{ass}^{triplex} \cdot mE2F1 \cdot miRNA_1 \cdot miRNA_2 - k_{deg}^{triplex} \cdot triplex - k_{dis}^{triplex} \cdot triplex \tag{S7}$$

The model accounts for the formation of two RNA duplexes (*duplex*) and one RNA triplex (*triplex*) involving E2F1 mRNA (*mE2F1*) and the two cooperating miRNAs (*miRNA$_1$* and *miRNA$_2$*) and the disassociation of these complexes as a result of reversible binding processes between miRNAs and the E2F1 mRNA. The rate constants $k_{prod}^{<E2F1,mE2F1,miRNA_1,miRNA_2>}$ represent the synthesis rates of E2F1 mRNA (k_{prod}^{mE2F1}) and protein (k_{prod}^{E2F1}) and the synthesis rates of *miRNA$_1$* ($k_{prod}^{miRNA_2}$) and *miRNA$_2$* ($k_{prod}^{miRNA_2}$). Synthesis of E2F1 protein (*E2F1*) depends on free *mE2F1*, and the syntheses of *mE2F1* and the two miRNAs depend on the transcriptional factors ($TF_{<mE2F1,miRNA_1,miRNA_2>}$) that induce their transcription. The rate constants $k_{ass}^{<duplex_1,duplex_2>}$ represent the association rates of duplexes, which are formed by *mE2F1* and

miRNA$_1$ (*duplex$_1$*) or *mE2F1* and *miRNA$_2$* (*duplex$_2$*). The respective dissociation rates are represented by $k_{dis}^{<duplex_1,duplex_2>}$. In case of the RNA triplex association and dissociation are represented by $k_{ass}^{triplex}$ and $k_{dis}^{triplex}$, respectively. All molecular species and complexes have a degradation term represented by $k_{deg}^{<\cdot>}$.

The parameter values were characterized as follows: The rate constants $k_{prod}^{<\cdot>}$, $k_{deg}^{<\cdot>}$ and $TF_{<\cdot>}$ were set to 1, making the nominal concentrations of *E2F1*, *mE2F1*, *miRNA$_1$* and *miRNA$_2$* equal to 1. Under this condition the concentrations of *E2F1* and *mE2F1* equal to 1 when none of the two miRNAs are expressed (i.e. no repression on E2F1 expression) and smaller than 1 otherwise. The association rates ($k_{ass}^{<\cdot>}$) were calculated using the equation $k_{ass}^{<duplex,triplex>} = \frac{EC(duplex,triplex)}{100\ nM}$, where *EC* represents the previously computed equilibrium concentrations of the complexes. For $k_{dis}^{<\cdot>}$, we used the minimum free energy (i.e. ΔG) computed by the NUPACK package (5). To make $k_{ass}^{<\cdot>}$ and $k_{dis}^{<\cdot>}$ comparable, we calculated $k_{dis}^{<\cdot>}$ using the equation $k_{dis}^{<duplex,triplex>} = \frac{\max(MFE(\cdot))}{MFE(duplex,triplex)}$, where $\max(MFE(\cdot))$ denotes the highest minimum free energy value (-2.68 kcal/mol; i.e. the most unstable complex) in the TriplexRNA database (2). The initial conditions of the model variables and the values of the model parameters are listed in Table S1 and S2.

To simulate E2F1 repression by cooperating miRNA pairs (Figure 3), we modulated $TF_{<miRNA>}$ in the interval [10^{-1} 10^{2}] to imitate the down- and upregulation of miRNA expression. We sampled 121*121 combinations of characteristic miRNA expression profiles in this interval and calculated the corresponding steady states of E2F1 ($SS_{E2F1}(TF_{miRNA_1}, TF_{miRNA_2})$). The gain of E2F1 repression efficiency for representative miRNA expression levels was calculated using the following equations and indicated as reference points in Figure 3:

(▲) $SS_{E2F1}(TF_{miRNA_1}=1, TF_{miRNA_2}=1)$ - $SS_{E2F1}(TF_{miRNA_1}=10, TF_{miRNA_2}=1)$;

(►) $SS_{E2F1}(TF_{miRNA_1}=1, TF_{miRNA_2}=1)$ - $SS_{E2F1}(TF_{miRNA_1}=1, TF_{miRNA_2}=10)$;

(♦) $SS_{E2F1}(TF_{miRNA_1}=1, TF_{miRNA_2}=1)$ - $SS_{E2F1}(TF_{miRNA_1}=5, TF_{miRNA_2}=5)$;

(●) $SS_{E2F1}(TF_{miRNA_1}=1, TF_{miRNA_2}=1)$ accounts for the steady state of E2F1 when the expression levels of both miRNAs are nominal.

$SS_{E2F1}(TF_{miRNA_1}=10, TF_{miRNA_2}=1)$ or $SS_{E2F1}(TF_{miRNA_1}=1, TF_{miRNA_2}=10)$ denotes the steady state of E2F1 when either miRNA is strongly upregulated. $SS_{E2F1}(TF_{miRNA_1}=5, TF_{miRNA_2}=5)$ indicates the steady state of E2F1 when both miRNAs are moderately upregulated.

To simulate cooperative repression of E2F1 by miR-205-5p and miR-342-3p in HC1299 and Sk-Mel-147 cells (Figure 4), we used their expression levels after plasmid transfection (Figure 4A) to characterize their transcriptional activation. More specifically, we normalized the expression levels of miR-205-5p and miR-342-3p in all 4 scenarios based on the control scenario (miR-Scr). The normalized miRNA expression levels were used to characterize the model parameters $TF_{<miR205,miR342>}$.

- For the H1299 cells, the values of $TF_{<miR205,miR342>}$ were set in different scenarios as follows: (i) transfection of a scrambled miRNA: TF_{miR205} =1, TF_{miR342} =1; (ii) transfection of miR-205-5p: TF_{miR205}=50, TF_{miR342}=1.02; (iii) transfection of miR-342-3p: TF_{miR205}=1, TF_{miR342}=46.19; and (iv) transfection of miR-205-5p and miR-342-3p: TF_{miR205}=25, TF_{miR342}=25.07.
- For the Sk-Mel-147 cells, the values of $TF_{<miR205,miR342>}$ in different scenarios were set as follows: (i) transfection of a scrambled miRNA: TF_{miR205} =1, TF_{miR342} =1; (ii) transfection of miR-205-5p: TF_{miR205}=15.68, TF_{miR342}=0.6; (iii) transfection of miR-

342-3p: TF_{miR205}=1.4, TF_{miR342}=4.23; and (iv) transfection of miR-205-5p and miR-342-3p: TF_{miR205}=3.23, TF_{miR342}=2.33.

Finally, we simulated the model and compared the steady states of *E2F1* and *mE2F1* with the experimental data that show the expression levels of E2F1 mRNA and protein in these scenarios (Figure 4D). Both the simulation results and the experimental data were normalized to the scenario in which a scrambled miRNA was transfected.

2.2. Kinetic modelling of chemoresistance and miRNA cooperativity

To simulate the effect of miR-205-5p and miR-342-3p on the response of tumour cells to drug treatment, we integrated the cooperative regulation of E2F1 by the two miRNAs into our previously published kinetic model of E2F1-mediated chemoresistance (Vera *et al.* 2013). The kinetic model is composed of thirteen ordinary differential equations, which account for the temporal dynamics of the regulatory network, whose activation is triggered after anticancer drug administration and modulates a phenotypic response in a population of tumour cells. The model has the following structure:

$$\frac{\partial mE2F1}{\partial t} = GxD \cdot k_1 + FS_{E2F1} \cdot k_2 - k_3 \cdot mE2F1 - k_4 \cdot miR205 \cdot mE2F1 - k_{33} \cdot miR342 \cdot mE2F1 - k_{34} \cdot miR205 \cdot miR342 \cdot mE2F1 \quad \text{(S8)}$$

$$\frac{\partial E2F1}{\partial t} = k_5 \cdot mE2F1 - k_6 \cdot E2F1 \quad \text{(S9)}$$

$$\frac{\partial p73}{\partial t} = k_7 \cdot E2F1 - k_8 \cdot p73 \quad \text{(S10)}$$

$$\frac{\partial DNp73}{\partial t} = k_9 \cdot E2F1 - k_{10} \cdot DNp73 \quad \text{(S11)}$$

$$\frac{\partial miR205}{\partial t} = k_{11} + \frac{k_{11} \cdot p73}{TGFB1} \cdot \left(1 + \frac{DNp73}{k_{13}}\right)^{-2} - k_{12} \cdot miR205 \quad \text{(S12)}$$

$$\frac{\partial miR342}{\partial t} = k_{35} \cdot FS_{miR342} - k_{36} \cdot miR342 \quad \text{(S13)}$$

$$\frac{\partial Bax}{\partial t} = k_{14} \cdot DS \cdot \frac{p73^{g_1}}{{k_{16}}^{g_1} + p73^{g_1}} \cdot \left(1 + \frac{DNp73}{k_{13}}\right)^{-2} - k_{15} \cdot Bax \quad \text{(S14)}$$

$$\frac{\partial Hrk}{\partial t} = k_{17} \cdot DS \cdot \frac{E2F1^{g_1}}{{k_{16}}^{g_1} + E2F1^{g_1}} - k_{18} \cdot Hrk \quad \text{(S15)}$$

$$\frac{\partial BCL2}{\partial t} = k_{19} \cdot \left(1 + \frac{miR205}{k_{20}}\right)^{-1} - k_{21} \cdot BCL2 \quad \text{(S16)}$$

$$\frac{\partial EGFR^*}{\partial t} = k_{25} \cdot GWF \cdot \left(\frac{E2F1^{g_2}}{{k_{32}}^{g_2} + E2F1^{g_2}} - EGFR^* - EGFR^i\right) - k_{26} \cdot EGFR^* \quad \text{(S17)}$$

$$\frac{\partial EGFR^i}{\partial t} = k_{27} \cdot CyD \cdot \left(\frac{E2F1^{g_2}}{{k_{32}}^{g_2} + E2F1^{g_2}} - EGFR^* - EGFR^i\right) \cdot \left(1 + \frac{ERBB3}{k_{37}}\right)^{-1} - k_{31} \cdot EGFR^i \quad \text{(S18)}$$

$$\frac{\partial ERBB3}{\partial t} = k_{29} \cdot \left(1 + \frac{miR205}{k_{30}}\right)^{-1} - k_{31} \cdot ERBB3 \quad \text{(S19)}$$

$$\frac{\partial TC}{\partial t} = k_{24} \cdot EGFR^* \cdot TC - k_{22} \cdot Hrk \cdot Bax \cdot \left(1 + \frac{BCL2}{k_{23}}\right)^{-1} \cdot TC \quad \text{(S20)}$$

Time dependent variables in the model account for the levels of: transcriptionally active E2F1 mRNA (*mE2F1*), E2F1 protein (*E2F1*), wild type p73 protein (*p73*), N-terminally truncated p73 isoform (DN*p73*), miR-205-5p (*miR205*), miR-342-3p (*miR342*), pro-apoptotic protein Harakiri (*Hrk*) and Bax (*Bax*), anti-apoptotic protein BCL2 (*BCL2*), active plasma membrane epidermal growth factor receptor EGFR ($EGFR^*$), drug-inhibited EGFR ($EGFR^I$), plasma membrane HER3 receptor (*ERBB3*), and the population of tumour cells whose phenotypic response after anticancer drug is mediated by the proposed network. Input variables in the model account for: dose of genotoxic drug (*GxD*), dose of cytostatic drug (*CyD*), expression level of the oncogenic protein TGFβ-1 (*TGFB1*), and the factors modulating the expression level of *mE2F1* (FS_{E2F1}) and *miR342* (FS_{miR342}).

Equations (S8-S13) account for the dynamics of the core regulatory signalling circuit of the model, composed of *E2F1*, *p73*, *DNp73*, *miR205*, and *miR342*. In the model, this subnetwork mediates the primary response to genotoxic drugs. In a nutshell, important regulatory processes included in this section of the model are the following: a) genotoxic-stress mediated E2F1 mRNA

synthesis (characterized by the parameters k_2, FS_{E2F1}, and k_1, and the input variable *GxD*), b) the repression of E2F1 mediated by individual miR-205-5p ((k_4) and miR-342 (k_{33}) or in a cooperative manner (k_{34}); and c) the regulation of miR-205-5p expression (k_{11}, k_{13}) by p73 (activator), DNp73 (repressor) and TGFβ-1 (repressor).

Equations (S14-S16) account for the transcriptional regulation of representatives of pro- and anti-apoptotic genes, whose expression is regulated upon genotoxic drug administration. The expression of Bax (*Bax*) is regulated by p73 and DNp73, Harakiri (*Hrk*) by E2F1 and BCL2 (*BCL2*) by miR-205-5p. Genotoxic drug-induced DNA damage signals (*DS*) can induce upregulation of pro-apoptotic genes *Hrk* and *BCL2*. **Equations (S17-S19)** account for the dynamics of expression and activity of the plasma membrane receptors EGFR ($EGFR^*$ and $EGFR^i$) and HER3 (*ERBB3*) in the context of E2F1 mediated proliferation and E2F1-mediated anticancer drug response. **Equations (S20)** accounts for the temporal dynamics of tumour cells (*TC*), whose proliferation and cell death after drug exposure are mediated by the regulatory network described in **Equations (S8-S19)**. In equation **(S13)** $EGFR^*$ connects the proliferation of the population to E2F1-related proliferative signals (k_{24}), while the E2F2 and p73 related pro- and anti-apoptotic proteins *Hrk, Bax*, and *BCL2* regulate the cell death rate after genotoxic stress at the population level (k_{22}, k_{23}). *GWF* accounts for genotoxic-drug mediated arrest of the tumour cell proliferation and thus determining whether or not the tumour cells can proliferate under certain biological conditions. The initial conditions of the model variables and the values of the model parameters can be found in Table S3 and S4.

Using the described model, we performed model simulations in which we iteratively modified the variables modulating the synthesis rates for the E2F1 mRNA (FS_{E2F1}) and the expression level of miR-342 (FS_{miR342}). To this end, the values of the corresponding model

parameters were iteratively modified in the interval [10^{-1}, 10^{2}] or [10^{-1}, 10^{4}] with respect to their nominal values in the Supplementary Table S4. Next, the network dynamics were simulated with the model, and protein expression levels, miR-205-5p levels, and the size of the tumour cell population were calculated in two different scenarios:

a) The non-drug stimulation condition is modelled by configuring specific model parameters as follows: *GxD*=0, *DS*=0 and *GWF*=1;
b) The genotoxic drug administration is modelled by configuring specific model parameters as follows: *GxD*=1, *DS*=1 and *GWF*=0, as such kind of drug can cause DNA damage that can lead to cell cycle arrest and thus preventing tumour cell from proliferating (6).

Figure 5C shows the steady states of the indicated model variables in the genotoxic drug administration. Figure 5D left shows the size of the tumour cell population (%) at 120 hr in the non-drug stimulation condition. Figure 5D right shows the size of the tumour cell population 24 hr after the drug administration. According to Vera *et al.* (7), in the non-drug condition the simulated cell population equal to or smaller than 150% of the initial cell population was considered not representative for tumour cells. Hence, their corresponding cell population variable (*TC*) was set to 0 (the cyan area in Figure 5D right). Otherwise, *TC* was set to the simulated values representing the surviving rate of the tumour cells in comparison to the initial population. By doing so, we visualized the effect of the genotoxic drug on tumour cells for different combinations of E2F1 and miR-342-3p expression.

3. RNA isolation and qPCR

RNA was extracted using the NucleoSpin RNA Kit (MACHEREY-NAGEL). For qRT-PCR, RNA was reverse transcribed with First Strand cDNA Synthesis Kit (Thermo Scientific). The cDNA samples were mixed with iQ™SYBR Green Supermix (Bio-Rad) and analyzed on iQ5™ Multicolor Real-Time PCR Detection System (Bio-Rad). Relative gene expression of E2F1 was

calculated by the comparative Ct method using GAPDH for normalization. PCR primers for detection of the specific DNA products are GAPDH-for: 5'-CAAGGT CATCCATGACAACTTTG-3'; GAPDH-rev: 5'-GTCCACCACCCTGTTGCTGTAG-3'; E2F1-for: 5'-GACCCTGACCTGCTGCTCT-3'; E2F1-rev: 5'-GGCCAGGTACTGATG GTCA-3'.

4. Supplementary table and figure

Table S1 The variables of the E2F1 model. The units of the model variables are arbitrary.

	$E2F1$	$mE2F1$	$miRNA_1$	$miRNA_2$	$duplex_1$	$duplex_2$	$Triplex$
Initial conditions	1	1	1	1	0	0	0

Table S2 The parameter of the E2F1 model. The units of the model parameters are arbitrary.

	$k_{ass}^{duplex_1}$	$k_{dis}^{duplex_1}$	$k_{ass}^{duplex_2}$	$k_{dis}^{duplex_2}$	$k_{ass}^{triplex}$	$k_{dis}^{triplex}$	$k_{prod}^{<\cdot>}, k_{deg}^{<\cdot>}, TF_{<\cdot>}$
miR-205-5p/miR-342-3p	0.0002	0.0948	0.0002	0.0885	0.9995	0.0530	
miR-205-5p/miR-377	0.5270	0.1182	0.0001	0.0841	0.4705	0.0598	
miR-205-5p/miR-152	0.3544	0.0880	0.0017	0.1157	0.6436	0.0627	1
miR-205-5p/miR-148a	0.0486	0.1044	0.0021	0.0880	0.9493	0.0592	
miR-205-5p/miR-148b	0.1092	0.0880	0.0020	0.1069	0.8888	0.0600	

Table S3 The variables of the chemoresistance model.

Variable	Description	Initial Condition (a.u.*)
mE2F1	E2F1 mRNA	1
E2F1	E2F1 protein	1
p73	Wild type p73 protein	1
DNp73	Mutated p73 protein	1
miR205	miR-205	1
miR342	miR-342	1
Bax	BAX protein	0
Hrk	pro-apoptotic protein Harakiri	0
BCL2	anti-apoptotic protein BCL2	1
EGFR*	Active Epithelial growth factor receptor	0
EGFR^i	Inactive Epithelial growth factor receptor	0
ERBB3	Receptor tyrosine-protein kinase ErbB-3	1
TC	Tumour cell population	1

*: arbitrary units.

Table S4 The parameters of the chemoresistance model.

Parameter	Description	Value	Comment
k_1	genotoxic stress mediated synthesis of E2F1 mRNA	20 hr^{-1}	assumed†
k_2	basal synthesis of E2F1 mRNA	2.085 hr^{-1}	Vera et al. 2013
k_3	basal degradation of E2F1 mRNA	0.139 hr^{-1}	Vera et al. 2013
k_4	miR-205 mediated repression of E2F1	0.01	Vera et al. 2013
k_5	mRNA-mediated synthesis of E2F1	0.231 hr^{-1}	Vera et al. 2013
k_6	basal degradation of E2F1	0.231 hr^{-1}	Vera et al. 2013
k_7	E2F1 mediated synthesis of p73	0.150 hr^{-1}	Vera et al. 2013
k_8	basal degradation of p73	1.386 hr^{-1}	Vera et al. 2013
k_9	E2F1 mediated synthesis of DNp73	0.1317hr^{-1}	Vera et al. 2013
k_{10}	basal degradation of DNp73	0.173 hr^{-1}	Vera et al. 2013
k_{11}	p73 mediated synthesis of miR-205	0.101 hr^{-1}	Vera et al. 2013
k_{12}	basal degradation of miR-205	0.029 hr^{-1}	Vera et al. 2013
k_{13}	threshold effective DNp73 repression of miR-205	10.267	Vera et al. 2013
k_{14}	p73 mediated synthesis of Bax	1 hr^{-1}	Vera et al. 2013
k_{15}	degradation rate of Bax	0.1 hr^{-1}	Vera et al. 2013
k_{16}	E2F1 level producing half maximum expression level for Hrk	16.899	Vera et al. 2013
k_{17}	E2F1 mediated synthesis of Hrk	0.1 hr^{-1}	Vera et al. 2013
k_{18}	degradation rate of Hrk	0.1 hr^{-1}	Vera et al. 2013
k_{19}	synthesis rate of BCL-2	0.03 hr^{-1}	Vera et al. 2013
k_{20}	threshold of miR-205-meidated repression of BCL2	5.560	Vera et al. 2013
k_{21}	degradation rate of BCL2	0.1 hr^{-1}	Vera et al. 2013
k_{22}	rate of apoptotic cells increase	1.0	Vera et al. 2013
k_{23}	threshold for effective anti-apoptotic gene expression	0.028 hr^{-1}	Vera et al. 2013
k_{24}	tumour size duplication time	0.0058 hr^{-1}	estimated*
k_{25}	growth factor mediated EGFR activation	2.773 hr^{-1}	Vera et al. 2013
k_{26}	active EGFR deactivation/degradation	0.693 hr^{-1}	Vera et al. 2013
k_{27}	cytostatic drug mediated inhibition of EGFR activation	0.693 hr^{-1}	Vera et al. 2013
k_{28}	drug-inhibited EGFR deactivation/degradation	0.0693 hr^{-1}	Vera et al. 2013
k_{29}	synthesis rate of ERBB3	0.277 hr^{-1}	Vera et al. 2013
k_{30}	threshold of miR-205-mediated repression of ERBB3	1	Vera et al. 2013
k_{31}	degradation rate of ERBB3	0.277 hr^{-1}	Vera et al. 2013

k_{32}	E2F1 level producing half maximum expression level for EGFR	7.071	Vera et al. 2013
k_{33}	miR-342 mediated repression of E2F1	0.01 hr^{-1}	assumed[††]
k_{34}	cooperative repression of E2F1 mediated by miR-342 and miR-205	0.02 hr^{-1}	assumed[††]
k_{35}	synthesis rate of miR-342	0.029 hr^{-1}	assumed for normalization
k_{36}	degradation rate of miR-342	0.029 hr^{-1}	assumed[†]
k_{37}	threshold for effective ERBB3-mediated inhibition of cytostatic drug	0.1	Vera et al. 2013
g_1	Hill coefficient	5.61	Vera et al. 2013
g_2	Hill coefficient	1.505	Vera et al. 2013
TGFB1	expression of oncogenic protein TGFB1	1	Vera et al. 2013
FS_{E2F1}	factors for modulating E2F1 expression	$[10^{-1}\ 10^{2}]$	tuneable[$]
FS_{miR342}	factors for modulating miR-342-3p expression	$[10^{-1}\ 10^{4}]$	tuneable[$]
DS	genotoxic drug mediated induction of pro-apoptotic genes	0 or 1	binary[#]
CyD	cytostatic drug mediated induction of EGFR inactivation	0	fixed[^]
GWF	genotoxic drug mediated arrest of tumour cell proliferation through EGFR	0 or 1	binary[#]

Model parameter values were taken from Vera *et al.* (2013) or in some cases derived from the analysis done in the present work. A detailed description on the model parameter values can be found in Vera *et al.* (2013). [*]This value is equivalent to the duplication time of tumour cells, which ranges from 96 hr and 500 days (8), and we used 5 days for the simulations. [†]The value is assumed based on the concentration of drug used in the experiments (Figure 6). [††]Based on the experimental data and simulation results (Figure 4), we assumed that the repression efficiency of E2F1 by miR-342-3p is similar to miR-205-5p and that their cooperative repression effects on E2F1 doubles compared to their individual repression. As the degradation rate of miR-324-3p is unknown we used the same value as miR-205-5p, assuming that it is a stable molecule based on the conclusion in (9). [$]Those parameters are sampled within the specified intervals for simulations. [#]Those parameters are binary and are set to 0 or 1 for corresponding biological conditions. [^]This parameter is set to 0 as in this study the effect of cytostatic drug is not considered.

Table S5 The used and estimated parameters for calculating the CI of the combined miRNA treatment in repressing E2F1.

Cell lines	D_{miR1} (μg)	D_{miR2} (μg)	$D_{\text{miR1+miR2}}$ (μg)	Median-effect doses of miRNAs	Kinetic order	Linear correlation	DRI_{miR1}	DRI_{miR2}
H1299	0.25	0.25	0.25 + 0.25	D^m_{miR1} = 0.468	m_{miR1} = 1.028	r_{miR1} = 0.957	2.023	3.438
H1299	0.5	0.5	0.5 + 0.5	D^m_{miR2} = 0.790	m_{miR2} = 0.961	r_{miR2} = 0.724	1.872	3.319
H1299	1	1	1 + 1	$D^m_{miR1+miR2}$ = 0.580	$m_{\text{miR1+miR2}}$ = 3.761	$r_{\text{miR1+miR2}}$ = 0.916	80.774	194.615
SK-Mel-147	0.25	0.25	0.25 + 0.25	D^m_{miR1} = 0.149	m_{miR1} = 1.811	r_{miR1} = 0.905	2.023	3.438
SK-Mel-147	0.5	0.5	0.5 + 0.5	D^m_{miR2} = 0.046	m_{miR2} = 0.654	r_{miR2} = 0.891	1.872	3.319
SK-Mel-147	1	1	1 + 1	$D^m_{miR1+miR2}$ = 0.080	$m_{\text{miR1+miR2}}$ = 1.896	$r_{\text{miR1+miR2}}$ = 0.991	80.774	194.615

The table shows the doses (*D*) of miRNAs used for calculating the combination indexes of the combined miRNA treatments in H1299 and SK-Mel-147 cells. The values of $D^m_{<miR1,miR2,miR1+miR2>}$ and $m_{<\text{miR1, miR2, miR1+miR2}>}$ were estimated by fitting the median-effect function to the experimental data (i.e. $D_{<miR1,miR2,\ miR1+miR2>}$ and their corresponding *fa*), and the linear correlation $r_{<\text{miR1, miR2, miR1+miR2}>}$ signifies the goodness of fit of the experimental data with the function (11). The dose-reduction index (*DRI*) is a measure of how many fold the dose of each miRNA in a synergistic combination may be reduced at a given effect level (11). The index is calculated using the equation $\frac{D^e_{miR}}{D_{miR}}$, where D_{miR} is the actual dose of a miRNA used in the combined miRNA treatment, and D^e_{miR} is the estimated dose of the miRNA that is needed to achieve the same effect, i.e. fa_{miR}, in the single miRNA treatment. If the value of $DRI_{<miR1,miR2>}$ is greater than 1, it indicates a dose reduction of a miRNA for repressing E2F1. miR1: miR-205; miR2: miR-342.

Table S6 The used and estimated parameters for calculating the CI of the combined miRNA treatment in chemosensitization of tumour cells.

D_{cDDP} (μM)	D_{miR1} (μg)	D_{miR2} (μg)	$D_{\text{miR1+miR2}}$ (μg)	Median-effect doses of miRNAs	Kinetic order	Linear correlation	DRI_{miR1}	DRI_{miR2}
20	0.5	0.5	0.25 + 0.25	D^m_{miR1} = 0.586	m_{miR1} = 5.542	r_{miR1} = 1	2.354	2.041
				D^m_{miR2} = 0.506	m_{miR2} = 3.190	r_{miR2} = 1		
20	1	1	0.5 + 0.5	$D^m_{miR1+miR2}$ = 0.499	$m_{\text{miR1+miR2}}$ = 16.57	$r_{\text{miR1+miR2}}$ = 1	9.349	37.347
40	0.25	0.25	0.125 + 0.125	D^m_{miR1} = 0.321	m_{miR1} = 3.572	r_{miR1} = 1	2.393	2.184
				D^m_{miR2} = 0.277	m_{miR2} = 19.444	r_{miR2} = 1		
40	0.5	0.5	0.25 + 0.25	$D^m_{miR1+miR2}$ = 0.267	$m_{\text{miR1+miR2}}$ = 4.114	$r_{\text{miR1+miR2}}$ = 1	2.658	1.265

The table shows the doses (*D*) of miRNAs used for calculating the combination indexes of the combined miRNA treatments in H1299 cells using different concentrations of cisplatin (20 μM or 40 μM). The detailed description of the parameters can be found in Table S5. miR1: miR-205; miR2: miR-342.

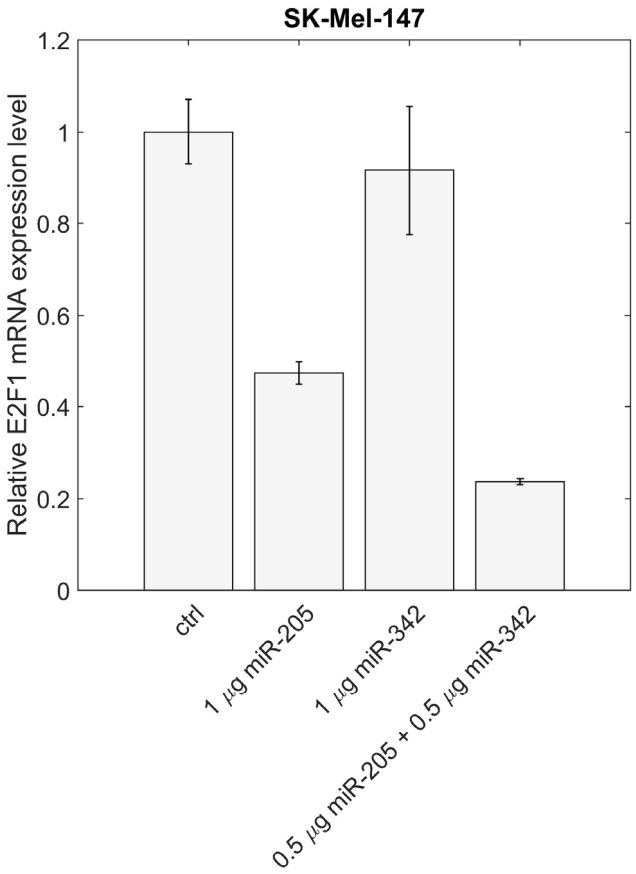

Figure S1 qPCR quantification of E2F1 mRNA expression using different miRNA treatments. The details of the experiments are described in the section of RNA isolation and qPCR in the Supplementary Materials. Data shown in the bar plots are mean ± SD (n = 3).

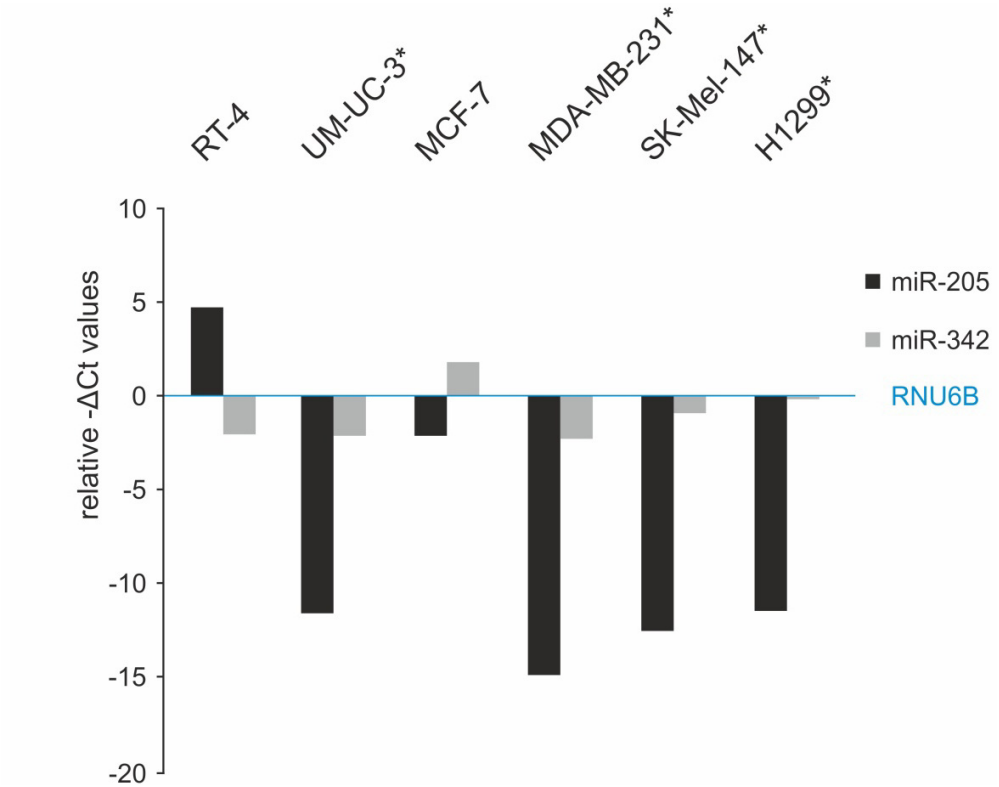

Figure S2 qPCR quantification of endogenous miR-205 and miR-342 expression in different aggressive cancer cell lines. The miRNA expressions are compared to the reference gene RNU6B. The status of endogenous miR-205-5p and miR-342-3p in various cell lines from different cancer types was determined by TaqMan qPCR. Differentially expressed miRNA levels are shown as -ΔCt values compared to RNU6B (set as 0). Asterisks indicate highly aggressive cell lines. RT-4, UM-UC-3 – bladder cancer; MCF-7, MDA-MB-231 – breast cancer; SK-Mel-147 – skin melanoma; H1299 – non-small cell lung cancer. Cells were obtained and cultured as described in our previous publication (10).

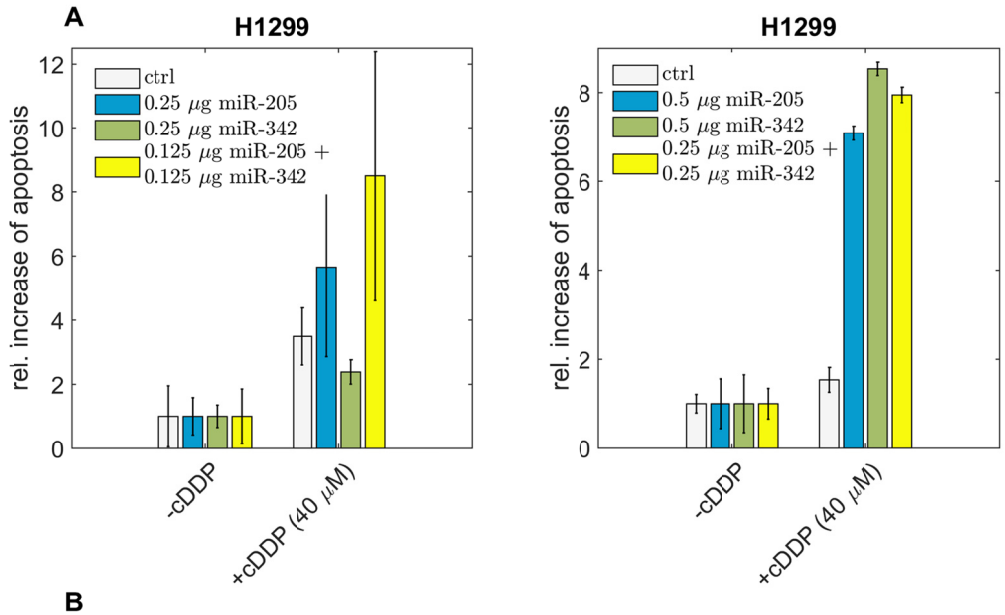

B

	fa_{miR205}	fa_{miR342}	$fa_{miR205+miR342}$	*CI*
40 µM (0.25 µg)	0.291	0.123	0.438	0.876
40 µM (0.5 µg)	0.830	0.999	0.931	1.167

Figure S3 (**A**) Cisplatin treatment (cDDP at 40 µM) of chemoresistant H1299 cells with single miR-205-5p (0.25 µg or 0.5 µg), miR-342-3p (0.25 µg or 0.5 µg) or combined miRNA (0.125 µg or 0.25 µg each) overexpression. Data shown in are mean ± SD (n=3). (**B**) The table shows the calculated fraction affected (*fa*) by the individual miRNA or combined miRNA treatments and the corresponding combination indexes (*CI*) of the combined treatments (synergism: $CI < 1$; antagonism: $CI > 1$). *fa* is denoted by relative increase of apoptosis of tumour cells that is normalized to the scenario with only drug treatment (i.e. ctrl in +cDDP) and further divided by the maximum increase of apoptosis in all listed treatments. Of note, when tumour cells were treated with 0.5 µg miR-342 the cells showed maximum increase of apoptosis in all scenarios listed in the table, therefore after normalization the corresponding *fa* should be 1. However, to calculate *CI* the interval of *fa* has to be constrained in (0, 1), so we set fa_{miR342} to 0.999.

5. References

1. Popenda,M., Szachniuk,M., Antczak,M., Purzycka,K.J., Lukasiak,P., Bartol,N., Blazewicz,J. and Adamiak,R.W. (2012) Automated 3D structure composition for large RNAs. *Nucleic Acids Res.*, **40**, e112.

2. Schmitz,U., Lai,X., Winter,F., Wolkenhauer,O., Vera,J. and Gupta,S.K. (2014) Cooperative gene regulation by microRNA pairs and their identification using a computational workflow. *Nucleic Acids Res.*, **42**, 7539–7552.

3. Foloppe,N. and MacKerell,A.D.J. (2000) All-Atom Empirical Force Field for Nucleic Acids : I . Parameter Optimization Based on Small Molecule and Condensed Phase Macromolecular Target Data. *J. Comput. Chem.*, **21**, 86–104.

4. MacKerell,A.D. and Banavali,N.K. (2000) All-atom empirical force field for nucleic acids: II. Application to molecular dynamics simulations of DNA and RNA in solution. *J. Comput. Chem.*, **21**, 105–120.

5. Zadeh,J.N., Steenberg,C.D., Bois,J.S., Wolfe,B.R., Pierce,M.B., Khan,A.R., Dirks,R.M. and Pierce,N.A. (2011) NUPACK: Analysis and design of nucleic acid systems. *J. Comput. Chem.*, **32**, 170–173.

6. Swift,L.H. and Golsteyn,R.M. (2014) Genotoxic anti-cancer agents and their relationship to DNA damage, mitosis, and checkpoint adaptation in proliferating cancer cells. *Int. J. Mol. Sci.*, **15**, 3403–3431.

7. Vera,J., Schmitz,U., Lai,X., Engelmann,D., Khan,F.M., Wolkenhauer,O. and Pützer,B.M. (2013) Kinetic modeling-based detection of genetic signatures that provide chemoresistance via the E2F1-p73/DNp73-miR-205 network. *Cancer Res.*, **73**, 3511–3524.

8. Corner,J. and Bailey,C.D. (2009) Cancer Nursing: Care in Context John Wiley & Sons.

9. Kai,Z.S. and Pasquinelli,A.E. (2010) MicroRNA assassins: factors that regulate the disappearance of miRNAs. *Nat. Struct. Mol. Biol.*, **17**, 5–10.

10. Khan,F.M., Marquardt,S., Gupta,S.K., Knoll,S., Schmitz,U., Spitschak,A., Engelmann,D., Vera,J., Wolkenhauer,O. and Pützer,B.M. (2017) Unraveling a tumor type-specific regulatory core underlying E2F1-mediated epithelial-mesenchymal transition to predict receptor protein signatures. *Nat. Commun.*, **8**, 198.

11. Chou,T.-C. (2006) Theoretical basis, experimental design, and computerized simulation of synergism and antagonism in drug combination studies. *Pharmacol. Rev.*, **58**, 621–681.